

Chemical Vapor Deposition of Photocatalytically Active Pure Brookite TiO₂ Thin films

Abdullah M. Alotaibi^a, Sanjayan Sathasivam^a, Benjamin A. D. Williamson^a, Andreas Kafizas^b, Carlos Sotelo-Vazquez^a, Alaric Taylor^c, David O. Scanlon^{a,d} and Ivan P. Parkin^{a*}

*Corresponding author

^aMaterials Chemistry Centre, Department of Chemistry, University College London,
20 Gordon Street, London WC1H 0AJ, UK

^bImperial College London, Department of Chemistry, South Kensington Campus,
London SW7 2AZ, U.K.

^cDepartment of Electronic & Electrical Engineering, University College London,
Torrington Place, London WC1E 7JE, UK

^dDiamond Light Source Ltd., Diamond House, Harwell Science and Innovation
Campus, Didcot, Oxfordshire OX11 0DE, United Kingdom.

Fax: (+44) 20-7679-7463

E-mail: i.p.parkin@ucl.ac.uk

Abstract

Brookite is the least investigated phase of TiO₂ due to the synthetic difficulty of obtaining the pure phase. Here, we present the first ever chemical vapour deposition synthesis of pure brookite TiO₂ thin films. The films were highly crystalline and phase pure as determined by X-ray diffraction and Raman spectroscopy studies. Scanning electron microscopy studies showed the films to have a structured morphology consisting of pyramidal features. The photocatalytic properties of the brookite film, tested using stearic acid under UVA (365 nm) irradiation, were superior to both an anatase film grown under similar conditions and NSG ActivTM glass. Transient absorption spectroscopy showed that the innate electron-hole recombination dynamics are similar in brookite and anatase, akin to previous reports. The superior

activity of the brookite film is hence attributed to the higher surface area compared to anatase.

Introduction

Titanium dioxide (TiO_2) is a well known, stable and highly versatile semiconductor.^{1,2} It is used for the purification of water and air through the photocatalytic degradation of organic compounds.^{3,4} Purification occurs under ultraviolet (UV) illumination where photoexcited electrons (in the conduction band) and holes (in the valence band) initiate the generation of reactive oxygen species (ROS) that react with and decompose organic pollutants.⁴ Furthermore, UV irradiation of TiO_2 also induces hydrophilicity of the surface therefore allowing application as self-cleaning and antifogging surfaces.

TiO_2 is commonly found in three crystal structures, the thermodynamically stable rutile (tetragonal) form and the metastable anatase (tetragonal) and brookite (orthorhombic) forms.⁵ Due to the ease of synthesis and natural abundance, the rutile and anatase phases have been prepared in both powder and thin film form by numerous routes and have been well investigated for numerous applications.⁶ With respect to the photocatalytic activity of the polymorphs, although it is somewhat controversial, the anatase phase is generally regarded as being more active than rutile.⁶⁻⁸ However, despite the comparatively fewer reports on brookite, some have reported higher photocatalytic activities than anatase, whereas other reports have shown it to be inactive for certain photocatalytic processes (*e.g.* the degradation of some dyes).⁹⁻¹² Hence the photoactivity of brookite remains a controversial issue that is not helped by the difficulty in producing phase pure samples in both powder and thin film form.^{9,13} As a result, it is difficult to determine whether the photocatalytic properties of the often rutile or anatase contaminated brookite samples are due to the innate activity of brookite, or synergetic effects due to the coupling of polymorphs (the most famous example being the synergetic interaction of anatase and rutile in the commercial photocatalyst P25 Degussa; often considered the benchmark photocatalyst).

In this paper, we demonstrate the first route to pure brookite thin films using chemical vapour deposition (CVD). The films have been characterized by XRD and Raman spectroscopy to determine phase purity. The photocatalytic activity of the brookite film was determined by measuring the degradation of stearic acid under 365 nm radiation and compared with an anatase film grown by CVD and a commercial self-

cleaning coating NSG ActivTM. Transient absorption spectroscopy (TAS) measurements were used to probe the kinetics of charge carrier recombination in the presence and absence of a hole scavenger (methanol). State of the art computational calculations were also used to give insight into the band structure of the CVD brookite film.

Experimental

Material and deposition procedure

Titanium butoxide [$\text{Ti}(\text{OCH}_2\text{CH}_2\text{CH}_2\text{CH}_3)_4$] (99%), methanol were purchased from Aldrich and used as received. Glass $150 \times 45 \times 40$ mm SiO_2 (50 nm) barrier coated float-glass was used as substrates to deposit the thin films. The glass plates were washed with acetone (99 %), isopropanol (99.9 %) and distilled water and dried in air prior to use. [$\text{Ti}(\text{OCH}_2\text{CH}_2\text{CH}_2\text{CH}_3)_4$] (0.5 g, 1.46 mmol) was dissolved in 20 ml of methanol in a glass bubbler. An aerosol mist generated using a Johnson Matthey Liquifog piezoelectric device. The mist was transferred to the reactor by nitrogen (BOC Ltd., 99.99%) with (flow rate 1.4 L min^{-1}) and the deposition was carried out at $550 \text{ }^\circ\text{C}$ for 40 mins. Post deposition the reactor was left to cool under N_2 to room temperature before films were removed. A $500 \text{ }^\circ\text{C}$ anneal step in air was carried out to remove any carbon contamination. A schematic of the set up is shown in Figure 1

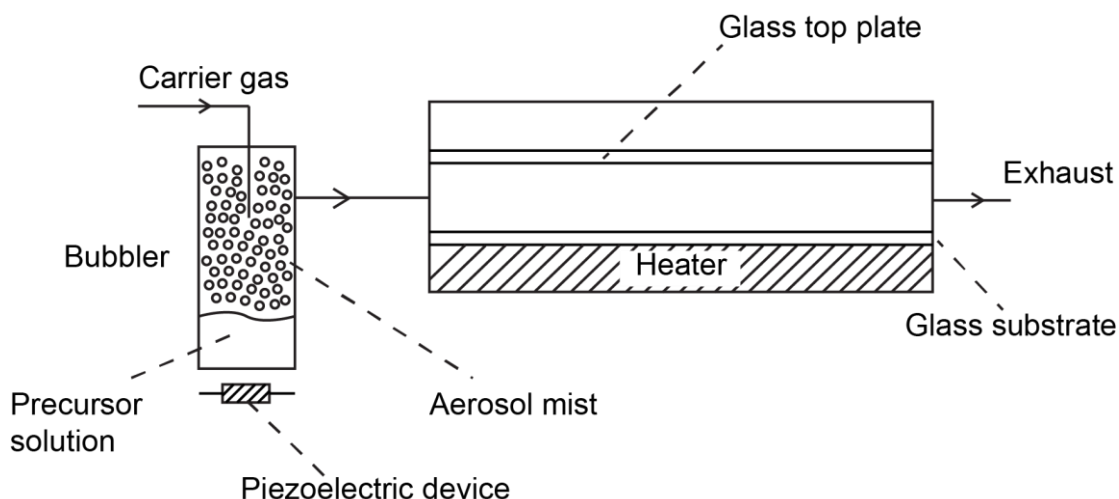


Figure 1: A schematic of the AACVD set up used to prepare the brookite thin films on glass substrates.

Film Characterisation

X-ray diffraction (XRD) patterns were measured in a modified Bruker-Axs D8 diffractometer with parallel beam optics and a PSD LynxEye silicon strip detector. This instrument uses an unmonochromated $\text{Cu K}\alpha$ source operated at 40 kV with 30 mA emission current. The incident beam angle was set at 0.5° and the angular range of the patterns collected was $10^\circ < 2\theta < 65^\circ$ with a step size of 0.05° counted at 1 s/step.

Scanning electron microscopy (SEM) was performed to determine surface morphology and film thickness using a JEOL JSM-6301F Field Emission SEM at an accelerating voltage of 5 keV.

Optical spectra were taken using a Perkin Elmer Fourier transform Lambda 950 spectrometer over a wavelength range of 190 nm to 2500 nm. This range encompasses the ultraviolet (UV), visible and near infrared (NIR) regions. The spectra were referenced against an air background.

X-ray photoelectron spectroscopy (XPS) was performed in a Thermo Scientific K-alpha photoelectron spectrometer using monochromatic Al-K_α radiation. Survey scans were collected in the range 0–1100 eV (binding energy) at a pass energy of 160 eV. Higher resolution scans were recorded for the main core lines at a pass energy of 20 eV. Valence band spectra were also recorded. Peak positions were calibrated to adventitious carbon (284.5 eV) and plotted using the CasaXPS software.

Computational Section

The Vienna *ab-initio* Simulation Package (VASP)^{14–17} was used to carry out hybrid density functional theory (hDFT) calculations on the electronic and structural properties of brookite TiO₂(*Pbca*). Hybrid functionals have been shown to accurately predict and describe the electronic structures of known structures in comparison to experiment^{18–24}, in particular, the HSE06^{25,26}(Heyd-Scuzeria-Ernzerhoff) functional has been known to describe the electronic properties of TiO₂ polymorphs well.^{2,27–31} HSE06 aims at solving the self-interaction error (SIE) inherent to standard functionals. The exchange interaction is split into a long range (LR) and short range (SR) part, with 25% of exact non-local Fock exchange substituting the short-range PBE (Perdew-Burke-Ernzerhoff)³² functional. The Coulomb potential is also split into long range and short range terms with a screening factor of 0.207 Å⁻¹ giving:

$$E_{xc}^{HSE0} = E_x^{HSE06,SR} + E_x^{PBE,LR} + E_c^{PBE}$$

Where

$$E_x^{HSE06,SR} = \frac{1}{4}E_x^{Fock,SR} + \frac{3}{4}E_x^{PBE,SR}$$

The Projector Augmented Wave Method (PAW)³³ was used in order to describe the interactions between the valence electrons and the core electrons (Ti:[Ar] and O[He]). A Γ -centred k-point mesh of 3x5x5 and a plane wave cutoff energy of 520eV was deemed to be sufficient for convergence for the 24 atom cell of brookite TiO₂ (shown in Figure 2). The structural optimisation carried out on the system involved a relaxation of the lattice vectors, cell angles, atomic positions and the cell volume. Convergence was deemed to be complete when the forces on all the atoms were less than 0.01eV \AA^{-1} . Following this, density of states (DOS) and band structure calculations were carried out. Valence band X-ray photoelectron spectroscopy (XPS) was simulated via weighting the calculated DOS using the atomic orbital photoionisation cross-sections formulated by Yeh and Lindau³⁴ which can be directly compared with experiment. In order to match the experimental broadening, a Gaussian broadening of 0.47eV was applied. This approach has displayed accurate accounts of the electronic states that make up the XPS data.^{24,35-38}

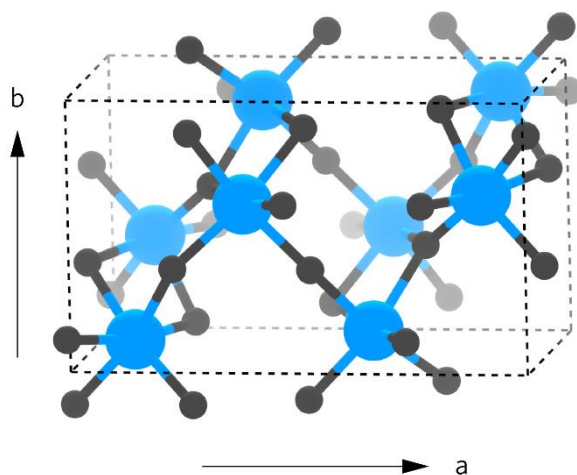


Figure 2: The unit cell of brookite - TiO₂(Pbca). The blue spheres represent Ti atoms and the dark grey spheres represent O atoms. The unit cell boundaries are shown with a dashed black line.

Photocatalytic activity

The films were cleaned in propan-2-ol, oven dried and coated with a stearic acid (0.05 M solution in chloroform) layer *via* dip coating. The photocatalytic activity of the films was monitored by Fourier transform-infrared (FT-IR) spectroscopy using a

PerkinElmer RX-I instrument. The IR spectrum of each acid-over layer was recorded over the range $3000 - 2700 \text{ cm}^{-1}$ and the areas of the peaks between 2950 and 2870 and 2870 and 2830 cm^{-1} integrated. Previously, Mills and Wang measured the change in area of the C-H stretches of stearic acid coatings using infrared spectroscopy (between $2700 - 3000 \text{ cm}^{-1}$).³⁹ They found a linear relationship between the area of the C-H stretches in stearic acid coatings, as measured by infrared spectroscopy, and the amount of stearic acid deposited ($9.7 \times 10^{15} \text{ molecules cm}^{-2} \equiv 1 \text{ A.cm}^{-1}$). Using this relationship, we were able to quantify the amount of stearic acid deposited onto our films by dip-coating, which showed little variation from sample to sample; ranging from 3.49 A.cm^{-1} on brookite to 3.65 A.cm^{-1} on the glass control (*i.e.* $\sim 3.4 \times 10^{16}$ molecules of stearic acid per cm^2 on brookite and $\sim 3.5 \times 10^{16}$ molecules of stearic acid per cm^2 on the glass control). Samples were irradiated using a 365 nm UVA lamp. At select intervals, the IR spectrum was recorded over the same range $3000 - 2700 \text{ cm}^{-1}$. Using the relationship above, the change in stearic acid was determined, and converted into a photocatalytic rate (stearic acid molecules degraded. $\text{cm}^{-2}.\text{s}^{-1}$).⁴⁰ The power of the UVA lamp was measured using a UVA radiometer equipped with a UVX-36 sensor ($I = 3.0 \text{ mW.cm}^{-2}$). The photon flux was determined ($\sim 5.5 \times 10^{15} \text{ photons.cm}^{-2}.\text{s}^{-1}$) and used to determine the formal quantum efficiency of the reaction (molecules of stearic acid degraded per incident photon).

Transient absorption spectroscopy

Transient absorption spectroscopy (TAS), from the microsecond to second timescale, was measured in either transmission or diffuse reflection mode. Brookite samples were highly scattering, and were measured in diffuse reflection mode. Anatase samples were highly transparent, and were measured in transmission mode. A Nd:YAG laser (OPOTEK Opolette 355 II, 7 ns pulse width) was used as the excitation source, generating 355 nm light from the third harmonic transmitted to the sample through a light guide ($\sim 6 \text{ ns}$ pulse width). An excitation power density of $\sim 1.5 \text{ mJ.cm}^{-2}$ and laser repetition rate of either 0.65 Hz or 0.35 Hz was used for measurements in argon or methanol degassed with argon respectively. As the photo-induced change in transmittance/ reflectance were low ($< 1\%$), we assumed that the transient signal was directly proportional to the concentration of excited species. The probe light was a 100 W Bentham IL1 quartz halogen lamp. Long pass filters (Comar Instruments) were placed between the lamp and sample to minimize short wavelength

irradiation of the sample. Diffuse reflectance from the sample was collected by a 2" diameter, 2" focal length lens and relayed to a monochromator (Oriel Cornerstone 130) to select the probe wavelength. Time-resolved intensity data was collected with a Si photodiode (Hamamatsu S3071). Data at times faster than 3.6 ms was recorded by an oscilloscope (Tektronics DPO3012) after passing through an amplifier box (Costronics), whereas data slower than 3.6 ms was simultaneously recorded on a National Instrument DAQ card (NI USB-6251). Each kinetic trace was obtained from the average of between 100 – 250 laser pulses. Acquisitions were triggered by a photodiode (Thorlabs DET10A) exposed to laser scatter. Data was acquired and processed using home-built software written in Labview.

Results and Discussion

Thin films of crystallographically pure brookite phase TiO₂ were synthesised by aerosol assisted chemical vapour deposition on glass substrates at 550 °C from the reaction of titanium butoxide (0.5 g, 1.46 mmol) and methanol (20 mL). It was found that the methanol was not only the solvent used to generate the aerosols but also an active reagent in the AACVD reaction. Depositions carried out under the same conditions, but with solvents such as toluene, hexane and ethanol produced only the expected anatase phase at the substrate temperature of 550 °C. Previous AACVD studies have found that the use of methanol as a solvent can produce unexpected results, for example Crick and Parkin found that the use of methanol and copper nitrate resulted in the formation of metallic Cu films whereas the use of other solvents (such as ethanol) produced Cu₂O and Cu-Cu₂O composite films.⁴¹ They attributed this observation to the *in situ* production of hydrogen catalyzed by the Cu films. From literature, almost all brookite formation has occurred via hydrothermal techniques and the mechanism for formation has not been resolved.⁴² There are reports that basic⁴³ and acidic^{42,44} conditions are necessary for successful brookite synthesis. From the AACVD results here, the mildly acidic conditions due to the methanol solvent may have helped to obtain phase pure films.

The brookite films were hazy white in appearance and well adhered to the substrate passing the Scotch™ tape test.⁴⁵

X-ray diffraction (XRD) performed on the films showed Bragg reflections between 10 and 65° 2 θ matching only the orthorhombic brookite crystal structure (JCPDS no. 29-1360) (Figure 3a) with texture coefficient calculations indicating a preference for growth in the (111) and (210) planes. Lattice parameters determined through HSE06 calculated results showed excellent agreement with literature results (< 0.4% difference) as shown in Table 1.⁴⁶

Table 1: The calculated HSE06 structural parameters for brookite TiO₂. Experimental results⁴⁶ are shown in brackets.

	a (Å)	b(Å)	c(Å)	$\alpha=\beta=\gamma$ (°)
TiO₂	9.21 (9.17)	5.46 (5.44)	5.15 (5.14)	90 (90)

It is important to note that the (210) and (111) reflections of brookite at 25.25° and 25.72° overlap heavily with the anatase (101) reflection 25.28°.⁴⁷ Therefore it can be difficult to determine phase purity from simply matching the collected data to the standard pattern XRD.

In addition to this, Raman spectroscopy, which is very sensitive to the presence of brookite, was used to remove any further doubt about the phase purity of the brookite films grown by CVD (Figure 3b). The Raman spectrum shows 15 vibrational bands that belong to the four (A_{1g}, B_{1g}, B_{2g} and B_{3g}) active modes of brookite.⁴⁸ No peaks corresponding to anatase or rutile were observed. In an effort to avoid any doubt, the A_{1g} peak observed in the brookite sample was modelled to determine the accurate peak position to be 151.00 cm⁻¹. This matches well with literature reports for the brookite principle A_{1g} band at 152 cm⁻¹.⁴⁹ The value, although close, is sufficiently different to the closest anatase band (E_g) that appears at 141 cm⁻¹.⁵⁰

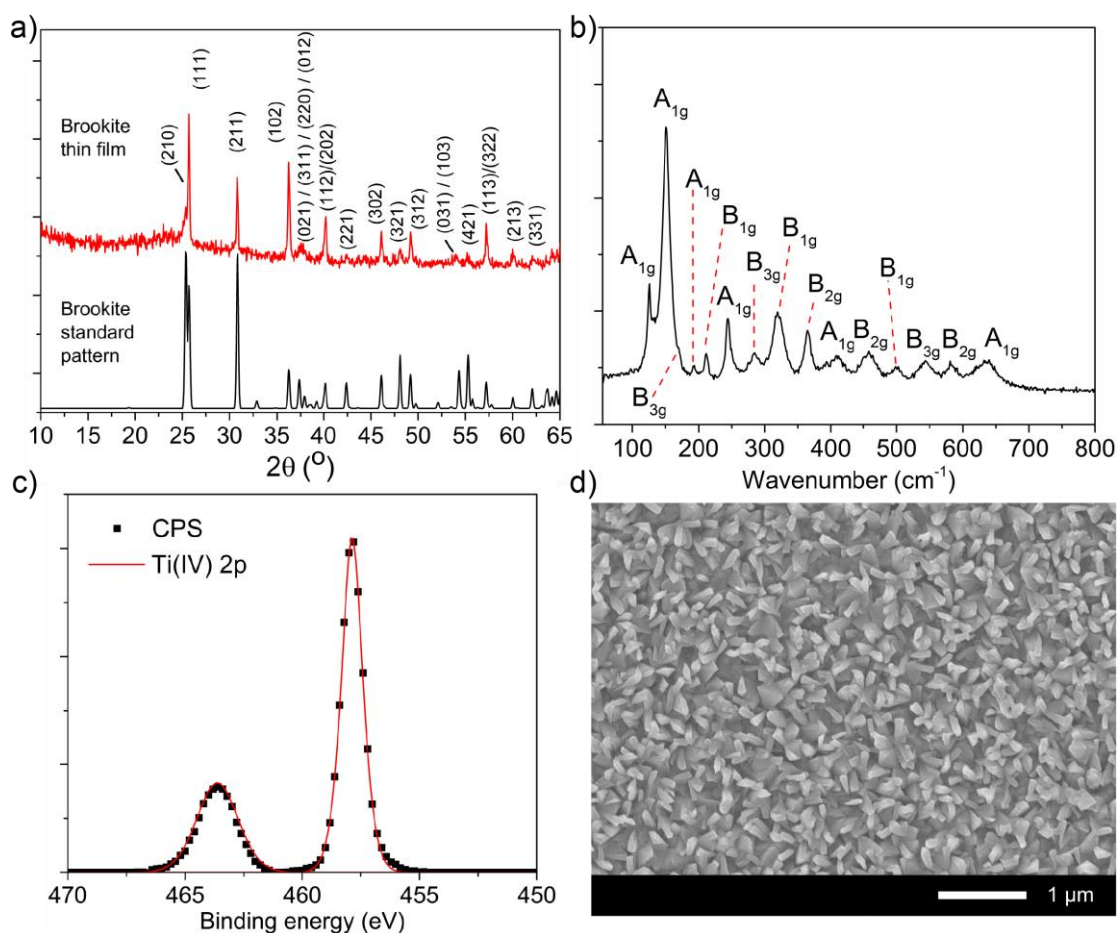


Figure 3: a) XRD, b) Raman, c) Ti 2p XPS spectrum and d) SEM image of the brookite phase thin film grown via AACVD.

X-ray photoelectron spectroscopy (XPS) showed the Ti 2p binding energies corresponded to Ti^{4+} , with the $2p_{3/2}$ and $2p_{1/2}$ peaks centered at 457.9 and 463.6 eV respectively (Figure 3c). No secondary peak for Ti^{3+} was observed.

The morphology of the film was seen *via* scanning electron microscopy (SEM) and is shown in Figure 3d. The surface of the brookite film is composed of narrow pyramidal features protruding from the substrate. This is different to the compact dome morphology typically observed in anatase TiO_2 grown by CVD. This is however very similar to the surface structure previously observed in TiO_2 - SnO_2 composite films grown by Carmalt *et al.*⁵¹

The protruding features observed in the brookite film are too small to scatter near infrared light as evidenced from UV-visible absorption spectroscopy (Figure 4a), and shows *ca.* 80% transmittance above 1500 nm. However, the features are large enough to scatter visible wavelengths, and hence shows a dip (down to 55%) in transmittance

in the visible region and thus explains the hazy white appearance of the films. The sharp drop in intensity at 365 nm corresponds to a direct band gap of 3.4 eV, as determined *via* a Tauc plot.

The calculated band structure for brookite is shown in Figure 4b and displays a direct band gap of 3.45 eV at the Γ point. This result is in excellent agreement to the experimental optical band gap determined for the AACVD grown brookite film. Furthermore the HSE06 calculated band gap is consistent with the range of band gap values seen in experiment (3.26-3.40 eV)^{6,27,47,52,53} (shown in Table 2) as well those seen in theory studies (2.38 – 3.86 eV)^{7,27,54,55}. The PBE^{7,55} (Perdew-Burke-Ernzerhoff)³² DFT results are the lowest of the calculated band gaps and the underestimation of the band gap is typical from this approach. The variation between the two different PBE studies is due to the use of DFT+U by Zhu et al.⁵⁵ where *U* refers to a Hubbard-like “U” parameter which introduces a penalty for partial occupation at a site. Interestingly from the three HSE06 results (this work included) no consistent agreement is seen between the band gaps. The explanations for the differing result from the work by Buckeridge et al.²⁷ is that experimentally determined lattice parameters and ionic positions were used in the analysis of the electronic properties of brookite, compared to a full ionic and volume optimisation carried out in this work. The 3.3 eV band gap calculated by Landmann et al.⁷ could be due to the use of a lower plane-wave energy cutoff. From all the methods tabulated in Table 2, the PBE + G_0W_0 (Green’s Function calculation of the electronic states on top of a structural optimisation carried out with PBE) matches our predicted band gap at 3.45 eV.

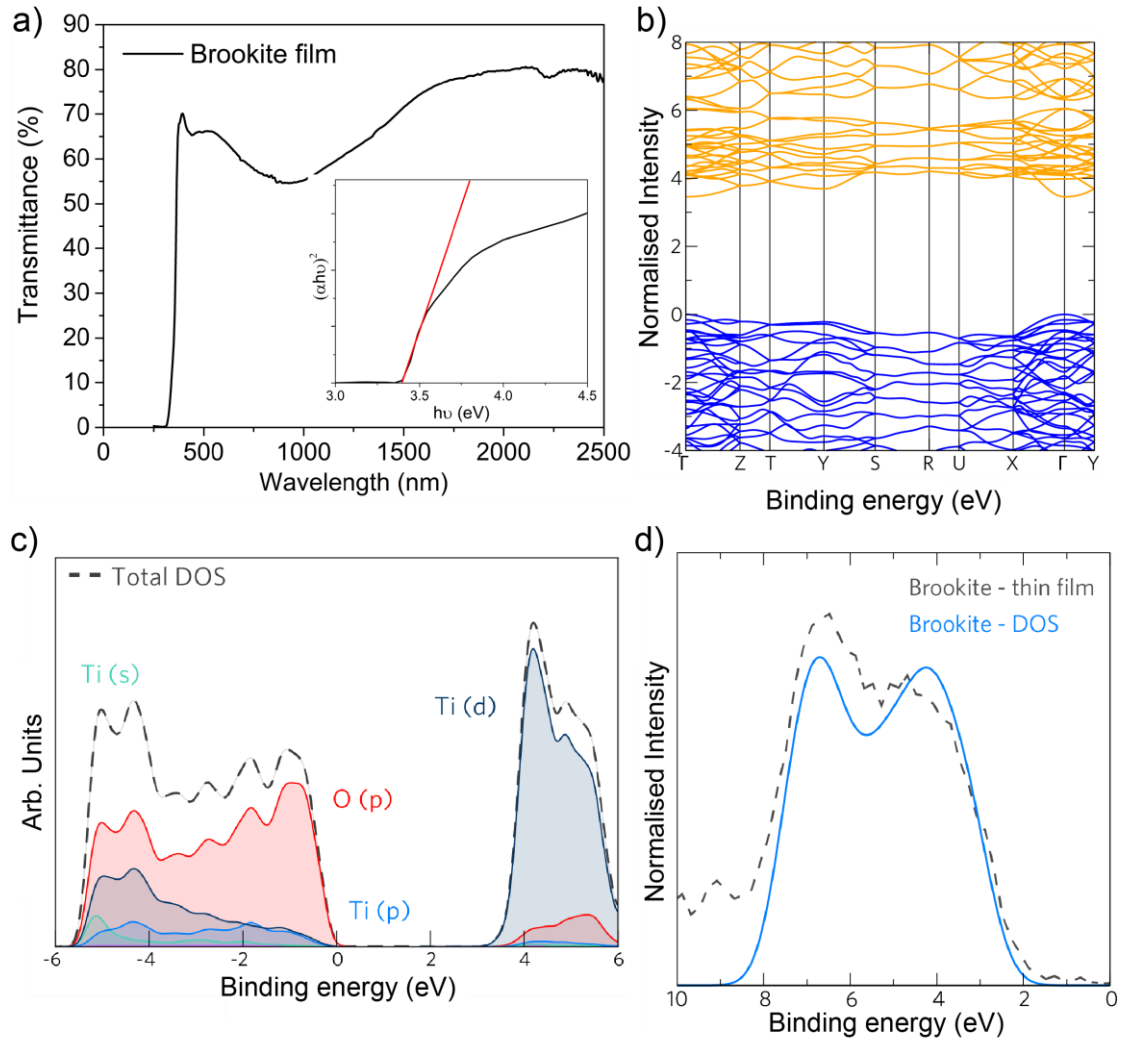


Figure 4: a) UV-vis spectrum (including Tauc plot as inset) and b) band structure using the hybrid HSE06 functional. The calculated c) Density of States (DoS) and d) the valence band XPS (VB-XPS) for brookite – TiO₂ with the simulated XPS overlaid in blue calculated with the HSE06 functional. In each diagram the valence band maximum (VBM) is set to 0 eV. In b) the valence band is coloured blue and the conduction band is coloured orange.

Table 2: Calculated and experimental band gaps from a range of techniques in the literature on brookite - TiO₂

Method	E _g (eV)
Extended Hückel Theory ⁵⁴	3.14
PBE (+U) ^{7,55}	1.86, 2.38
PBE + G ₀ W ₀ ⁷	3.45
HSE06 ^{7,27}	3.30, 3.51
HSE06 + G ₀ W ₀ ⁷	3.68
GW ⁵⁵	3.86

<i>This work</i>	3.45
Experiment ^{6,47,52,53}	3.26, 3.29, 3.31, 3.4

The electronic density of states (DoS) for brookite is shown in Figure 4c. As with all polymorphs of TiO₂, the valence band maximum (VBM) is primarily dominated by O *p* states mixing with negligible Ti *p* and *d* states (~ 4%) whereas the conduction band minimum (CBM) is made up of Ti *d* states (~ 96%) with minimal O states. These results are consistent with previous DFT calculations on brookite and TiO₂ polymorphs.^{2,27} The simulated valence band XPS (VB-XPS) weighted using the atomic orbital photoionisation cross-sections formulated by Yeh and Lindau³⁴ is shown alongside the experimentally determined VB-XPS in Figure 4d. The simulated data is in excellent agreement with the experimental data displaying a peak width of ~ 6 eV with a small trough at ~ 5.5 eV corresponding to a lack of density of states at that region.

Interest in brookite as a water splitting photocatalyst has grown, and can be attributed to the favourable positions of its band edges with respect to the redox potentials of water. A comparison with the other polymorphs of TiO₂ shows that brookite has a CBM higher in energy than both anatase, rutile and (more importantly) the reduction potential of water (H₂/H₂O).^{27,47,56}

The photocatalytic properties of the brookite film was measured under UVA (365 nm) illumination ($I = 3.0 \text{ mW.cm}^{-2}$) for the degradation of stearic acid (Figure 5a). Stearic acid is a widely used and the preferred method to determine the photocatalytic activity of photocatalytic films.³⁹ This is due to its stability under UV irradiation and a model compound for solid films that form on exterior and interior surfaces.³⁹

A stearic acid destruction rate of $3.31 \times 10^{-4} \text{ A.cm}^{-1}.\text{s}^{-1}$ was calculated from the reduction in area of the characteristic C-H stretches observed over the 2700 – 3000 cm⁻¹ range with irradiation time. A control glass slide coated with stearic acid was also tested to take into consideration any loss of stearic acid that may be caused by evaporation or photo-induced degradation; no significant change in stearic acid concentration was found on the control, similar to previous observations by Mills and Wang.³⁹ The brookite film showed a formal quantum efficiency of 5.81×10^{-4}

molecules per incident photon (Figure 5b). As each photon creates two charges (an electron and a hole), that can either directly or indirectly degrade stearic acid (*via* radicals *etc*), and given stearic acid takes 104 electron transfers for each molecule to be degraded, this means that the FQE of brookite can be expressed as $5.81 \times 10^{-4} \times (104/2) = 3.02 \times 10^{-2}$ charges that take part in photocatalysis per incident photon or rather, 3.02 % of charges take part in photocatalysis per 100 incident photons. The brookite film was almost four times superior than an anatase film (1.17×10^{-4} molecules per incident photon) grown under similar conditions. Furthermore, the brookite film showed more than twice the activity than commercial self-cleaning glass (2.64×10^{-4} molecules per incident photon), NSG ActivTM – the industry benchmark thin film photocatalyst that is often used as a comparison when investigating the photocatalytic properties of thin films.

To our knowledge, the precise mechanism by which stearic acid is photocatalytically degraded by TiO₂ is not known. As such, a general photocatalytic mechanism is assumed, whereby photo-generated holes oxidize surface bound OH groups, or water, to hydroxyl radicals (OH[•]) and photo-generated electrons reduce di-oxygen into superoxide (O₂^{•-}), which may further react with water to form a range of radical species and compounds (such as HO₂[•], HO₂⁻, H₂O₂ and possibly OH[•]).⁵⁷ These radicals, formed on the surface of TiO₂ under ambient conditions in the presence of UV light, can oxidize organic matter in the vicinity of TiO₂ into mineral acids and carbon dioxide (when oxidized to completion).

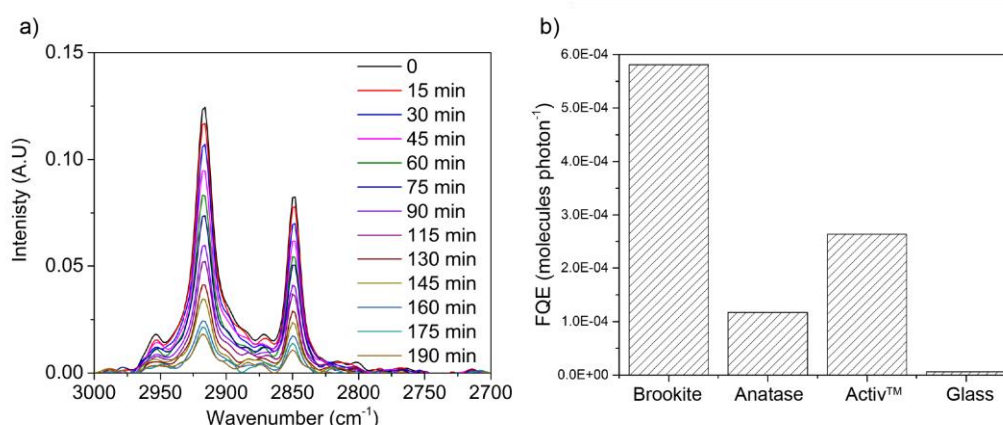


Figure 5: a) degradation of stearic acid on brookite TiO₂ b) the formal quantum efficiencies for the destruction of stearic acid on brookite, anatase, NSG ActivTM and a glass control.

TiO₂ anatase and rutile phases are well known for their photoinduced superhydrophilicity (Figure 6). Surprisingly the brookite film showed a remarkably low contact angle with water prior to any irradiation, whereas the anatase film grown under similar conditions showed the expected ca. 70° for TiO₂ prior to UVA irradiation. Non-UV irradiation induced superhydrophilicity has been observed previously for TiO₂ systems with many finding the surface roughness of the films to be the primary cause.^{58–60} This is possibly the case here too, with the natural hydrophilicity of the brookite film further enhanced by the high surface roughness.

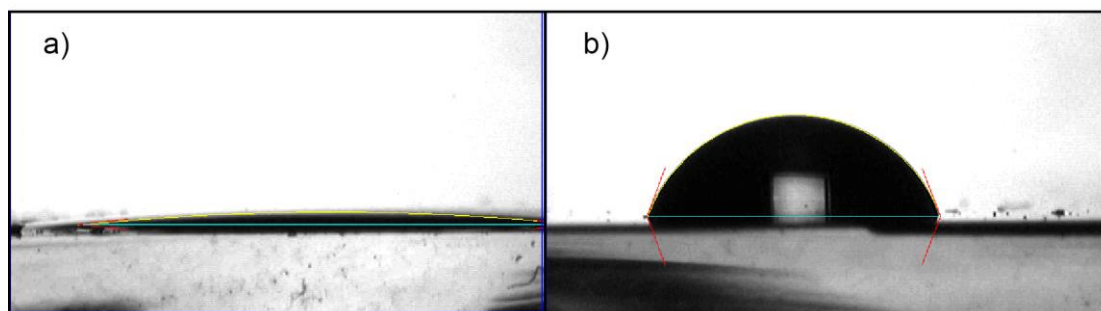


Figure 6: The water contact angle on a) brookite b) anatase TiO₂ thin films grown under via AACVD prior to any irradiation with a light source.

Transient absorption spectroscopy (TAS) is a form of laser flash spectroscopy that can be used to monitor the generation, recombination, trapping and charge transfer events of photo-generated charges in semiconductors.⁶¹ The dynamics specific to photo-generated electrons or holes can be studied by tracking transient changes in absorbance at particular wavelengths.⁴ Using TAS, we measured the innate charge carrier recombination dynamics of brookite in argon, as well as the reactivity of holes with a scavenger; methanol. The kinetics of the reaction of photo-generated holes with methanol⁶² is several orders of magnitude faster than their reaction with water⁴; therefore, hole scavenging more effectively competes, and thereby inhibits, electron-hole recombination. This has been used to great effect in studying the water splitting reaction on colloidal photocatalysts, where methanol is used as a chemical scavenger of holes, allowing photo-generated electrons to reduce water to form hydrogen.⁶³

The electron-hole recombination dynamics in brookite, and spectral features (Figure S4), were similar to previous studies of mesoporous films of brookite,⁶⁴ where electron-hole recombination showed a $t_{50\%}$ (time to reach 50% of the signal from the start of the measurement; 10 μ s) of $\sim 100 \mu$ s. The recombination kinetics in our

anatase film were measured for comparison (Figure S5). Analogous to brookite, our anatase samples showed a $t_{50\%}$ of ~ 100 μs , which showed that electron-hole recombination in these two distinct polymorphs occurs at a similar rate. However, when the hole scavenger methanol was added, a substantial effect was only observed in our brookite sample (Figure 7). This resulted in a longer lived signal, attributed to concomitant electron carriers that remain in the material. No significant hole scavenging effect was observed in our anatase sample. We should make it clear that this was not because holes in anatase cannot be scavenged strongly by methanol, indeed they can, where nanopowders or mesoporous structures often show a strong hole scavenging effect.^{62,64,65} However, in the case of a flat and dense sample, the quantum yield of this interaction is too low to see a hole scavenging effect (as bulk electron-hole recombination dominates).⁶⁵

Overall, our TAS results show that the innate electron-hole recombination dynamics are similar in brookite and anatase, akin to previous reports.^{64,66} Therefore, the higher photocatalytic activity of our brookite sample cannot be attributed to an innate increase in charge carrier lifetime compared with anatase. Rather, owing to the higher surface area and nanostructure of brookite, a higher proportion of charge carriers are generated at the surface, and can react with species at the surface (*i.e.* methanol in the case of our TAS experiments). In the case of anatase, its highly flat and densely packed structure meant that a high proportion of charge carriers were formed in the bulk, which cannot reach the surface and react (due, in part, to the poor mobility of holes in TiO_2).⁶¹ Atomic force microscopy (AFM) measurements did indeed show the surface area of the brookite film to be larger at 44.5 μm^2 compared to the 29.1 μm^2 measured for anatase (Figure S6).

Previous studies have shown that stearic acid is completely photocatalytically oxidized into carbon dioxide and water on TiO_2 surfaces.⁴⁰ The FQE observed in the photocatalytic oxidation of stearic acid on our brookite films was approximately $\sim 3\%$ per incident photon, which means that $\sim 97\%$ of photo-generated charges recombine before taking part in photocatalysis. This can be attributed to the competing timescales of electron-hole recombination, and the formation of radicals at the surface of TiO_2 through reactions of photo-generated charges with water and oxygen.⁵⁷ Our transient absorption spectroscopy studies showed electron-hole recombination occurred with a $t_{50\%}$ of ~ 100 μs , measured from 10 μs , in both anatase and brookite.

Previous studies of anatase TiO₂ show that photo-generated electrons react with oxygen on the ms timescale,⁶⁷ and photo-generated holes react with water on a similarly slow timescale.⁴ As electron-hole recombination occurs on faster timescales than the reaction of photo-generated charges to form surface radicals, recombination dominates; resulting in the low FQEs observed herein. However, it should be noted that the films studied herein show more than double the FQE previously observed by Kafizas *et. al.* for anatase TiO₂ films grown using a sol-gel route (FQE $\sim 2.4 \times 10^{-4}$ molecules per incident photon).⁶⁸

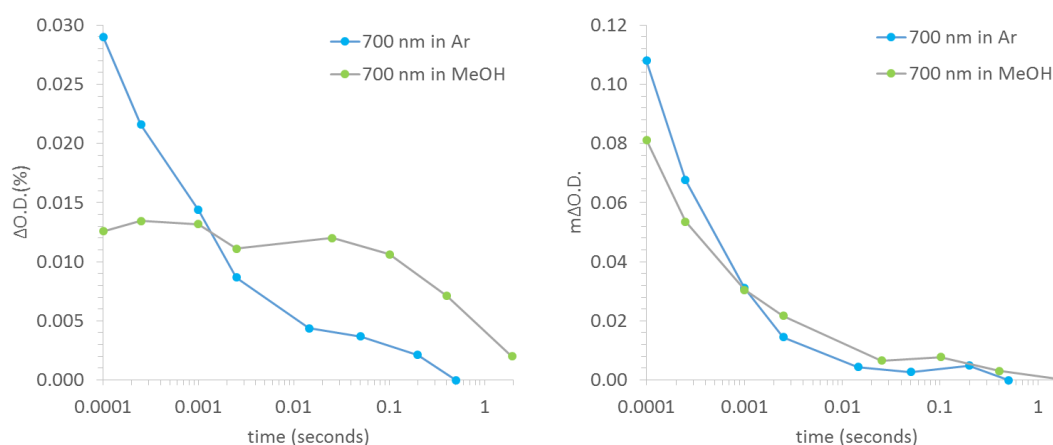


Figure 7: Transient absorption decays in brookite (left) and anatase (right) in argon (Ar) or methanol (MeOH). Decays were measured at a probe wavelength of 700 nm, 100 μ s after a laser pulse (laser = 355 nm, $\sim 1.5 \text{ mJ.cm}^{-2}$ per pulse, 6 ns pulse width).

Conclusion

In this paper, phase pure brookite TiO₂ films synthesized via CVD were tested for their material and photocatalytic properties. The brookite films showed superior photocatalytic activity in the destruction of stearic acid compared to an anatase film grown under similar conditions and to NSG Activ. As TAS results showed that since the electron-hole recombination dynamics are similar in both brookite and anatase the higher photocatalytic activity of brookite was attributed to the more structured morphology giving rise to a higher surface area. State of the art hybrid density functional theory calculations revealed a direct band gap for brookite at 3.45 eV which matched well with experimental results (3.4 eV).

Acknowledgment

The authors would like to thank Dr. Steve Firth for assistance with SEM imaging. Professor James R. Durrant is thanked for useful discussions and for providing access to the TAS instruments. We are grateful to King Abdulaziz City for Science and Technology (KACST), Saudi Arabia for the provision of a Ph.D studentship to A.M.A. The Saudi Cultural Bureau in London is also thanked by A.M.A for financial support.

Supporting information

Anatase TiO₂ XRD and SEM, TAS and AFM for brookite and anatase

References

- (1) Linsebigler, A. L.; Lu, G.; Yates Jr, J. T. Photocatalysis on TiO₂ Surfaces: Principles, Mechanisms, and Selected Results. *Chem. Rev.* **1995**, *95* (3), 735–758.
- (2) Scanlon, D. O.; Dunnill, C. W.; Buckeridge, J.; Shevlin, S. A.; Logsdail, A. J.; Woodley, S. M.; Catlow, C. R. A.; Powell, M. J.; Palgrave, R. G.; Parkin, I. P.; Watson, G. W.; Keal, T. W.; Sherwood, P.; Walsh, A.; Sokol, A. A. Band Alignment of Rutile and Anatase TiO₂. *Nat. Mater.* **2013**, *12*, 798–801.
- (3) Fujishima, A. Electrochemical Photolysis of Water at a Semiconductor Electrode. *Nature* **1972**, *238*, 37–38.
- (4) Fujishima, A.; Zhang, X.; Tryk, D. TiO₂ Photocatalysis and Related Surface Phenomena. *Surf. Sci. Rep.* **2008**, *63*, 515–582.
- (5) Mo, S.-D.; Ching, W. Y. Electronic and Optical Properties of Three Phases of Titanium Dioxide: Rutile, Anatase, and Brookite. *Phys. Rev. B* **1995**, *51*, 13023.
- (6) Shibata, T.; Irie, H.; Ohmori, M.; Nakajima, A.; Watanabe, T.; Hashimoto, K. Comparison of Photochemical Properties of Brookite and Anatase TiO₂ Films. *Phys. Chem. Chem. Phys.* **2004**, *6*, 1359.
- (7) Landmann, M.; Rauls, E.; Schmidt, W. G. The Electronic Structure and Optical Response of Rutile, Anatase and Brookite TiO₂. *J. Phys. Condens. Matter* **2012**, *24*, 195503.
- (8) Zhang, J.; Zhou, P.; Liu, J.; Yu, J. New Understanding of the Difference of Photocatalytic Activity among Anatase, Rutile and Brookite TiO₂. *Phys. Chem. Chem. Phys.* **2014**, *16*, 20382–20386.
- (9) Lin, H.; Li, L.; Zhao, M.; Huang, X.; Chen, X.; Li, G.; Yu, R. Synthesis of High-Quality Brookite TiO₂ Single-Crystalline Nanosheets with Specific Facets Exposed: Tuning Catalysts from Inert to Highly Reactive. *J. Am. Chem. Soc.* **2012**, *134*, 8328–8331.
- (10) Li, J.-G.; Ishigaki, T.; Sun, X. Anatase, Brookite, and Rutile Nanocrystals via Redox Reactions under Mild Hydrothermal Conditions: Phase-Selective

- Synthesis and Physicochemical Properties. *J. Phys. Chem. C* **2007**, *111*, 4969–4976.
- (11) Zhao, B.; Chen, F.; Huang, Q.; Zhang, J. Brookite TiO₂ Nanoflowers. *Chem. Commun.* **2009**, No. 34, 5115–5117.
- (12) Li, G.; Gray, K. A. Preparation of Mixed-Phase Titanium Dioxide Nanocomposites via Solvothermal Processing. *Chem. Mater.* **2007**, *19*, 1143–1146.
- (13) Kuznetsova, I. N.; Blaskov, V.; Stambolova, I.; Znaidi, L.; Kanaev, A. TiO₂ Pure Phase Brookite with Preferred Orientation, Synthesized as a Spin-Coated Film. *Mater. Lett.* **2005**, *59*, 3820–3823.
- (14) Kresse, G.; Hafner, J. Ab Initio Molecular Dynamics for Liquid Metals. *Phys. Rev. B* **1993**, *47*, 558–561.
- (15) Kresse, G.; Hafner, J. Ab-Initio Molecular-Dynamics Simulation of the Liquid-Metal Amorphous-Semiconductor Transition in Germanium. *Phys. Rev. B* **1994**, *49*, 14251–14269.
- (16) Kresse, G.; Furthmüller, J. Efficiency of Ab-Initio Total Energy Calculations for Metals and Semiconductors Using a Plane-Wave Basis Set. *Comput. Mater. Sci.* **1996**, *6*, 15–50.
- (17) Kresse, G.; Furthmu, J.; J., F.; Kresse, G.; Furthmu, J. Efficient Iterative Schemes for Ab Initio Total-Energy Calculations Using a Plane-Wave Basis Set. *Phys. Rev. B Condens. Matter Mater. Phys.* **1996**, *54*, 11169.
- (18) Burbano, M.; Scanlon, D. O.; Watson, G. W. Sources of Conductivity and Doping Limits in CdO from Hybrid Density Functional Theory. *J. Am. Chem. Soc.* **2011**, *133*, 15065–15072.
- (19) Rajpalke, M. K.; Linhart, W. M.; Birkett, M.; Yu, K. M.; Scanlon, D. O.; Buckeridge, J.; Jones, T. S.; Ashwin, M. J.; Veal, T. D. Growth and Properties of GaSbBi Alloys. *Appl. Phys. Lett.* **2013**, *103*, 0–4.
- (20) Zhang, S. B.; Northrup, J. E. Chemical Potential Dependence of Defect Formation Energies in GaAs: Application to Ga Self-Diffusion. *Phys. Rev. Lett.*

- 1991**, 67, 2339.
- (21) Ganose, A. M.; Savory, C. N.; Scanlon, D. O. $(\text{CH}_3\text{NH}_3)_2\text{Pb}(\text{SCN})_2$: A More Stable Structural Motif for Hybrid Halide Photovoltaics? *J. Phys. Chem. Lett.* **2015**, 6, 4594–4598.
- (22) Walsh, A.; Chen, S.; Wei, S. H.; Gong, X. G. Kesterite Thin-Film Solar Cells: Advances in Materials Modelling of $\text{Cu}_2\text{ZnSnS}_4$. *Adv. Energy Mater.* **2012**, 2, 400–409.
- (23) Kehoe, A. B.; Temple, D. J.; Watson, G. W.; Scanlon, D. O. Cu_3MCh_3 (M = Sb, Bi; Ch = S, Se) as Candidate Solar Cell Absorbers: Insights from Theory. *Phys. Chem. Chem. Phys.* **2013**, 15, 15477–15484.
- (24) Marchand, P.; Sathasivam, S.; Williamson, B. A. D.; Pugh, D.; Bawaked, S. M.; Basahel, S. N.; Obaid, A. Y.; Scanlon, D. O.; Parkin, I. P.; Carmalt, C. J. A Single-Source Precursor Approach to Solution Processed Indium Arsenide Thin Films. *J. Mater. Chem. C* **2016**, 4, 6761–6768.
- (25) Heyd, J.; Scuseria, G. E.; Ernzerhof, M. Hybrid Functionals Based on a Screened Coulomb Potential. *J. Chem. Phys.* **2003**, 118, 8207–8215.
- (26) Paier, J.; Marsman, M.; Hummer, K.; Kresse, G.; Gerber, I. C.; Angyán, J. G.; Screened Hybrid Density Functionals Applied to Solids. *J. Chem. Phys.* **2006**, 124, 154709.
- (27) Buckeridge, J.; Butler, K. T.; Catlow, C. R. A.; Logsdail, A. J.; Scanlon, D. O.; Shevlin, S. A.; Woodley, S. M.; Sokol, A. A.; Walsh, A. Polymorph Engineering of TiO_2 : Demonstrating How Absolute Reference Potentials Are Determined by Local Coordination. *Chem. Mater.* **2015**, 27, 3844–3851.
- (28) Çelik, V.; Mete, E. Range-Separated Hybrid Exchange-Correlation Functional Analyses of Anatase TiO_2 Doped with W, N, S, W/N, or W/S. *Phys. Rev. B - Condens. Matter Mater. Phys.* **2012**, 86, 1–9.
- (29) Huy, H. A.; Aradi, B.; Frauenheim, T.; Deák, P. Calculation of Carrier-Concentration-Dependent Effective Mass in Nb-Doped Anatase Crystals of TiO_2 . *Phys. Rev. B* **2011**, 83, 155201.

- (30) Janotti, A.; Varley, J. B.; Rinke, P.; Umezawa, N.; Kresse, G.; Van de Walle, C. G. Hybrid Functional Studies of the Oxygen Vacancy in TiO₂. *Phys. Rev. B* **2010**, *81*, 85212.
- (31) Bhachu, D. S.; Sathasivam, S.; Sankar, G.; Scanlon, D. O.; Cibin, G.; Carmalt, C. J.; Parkin, I. P.; Watson, G. W.; Bawaked, S. M.; Obaid, A. Y.; Al-Thabaiti, S.; Basahel, S. N. Solution Processing Route to Multifunctional Titania Thin Films: Highly Conductive and Photocatalytically Active Nb:TiO₂. *Adv. Funct. Mater.* **2014**, *24*, 5075–5085.
- (32) Perdew, J. P.; Burke, K.; Ernzerhof, M. Generalized Gradient Approximation Made Simple. *Phys. Rev. Lett.* **1996**, *77*, 3865–3868.
- (33) Blochl, P. E. Projector Augmented-Wave Method. *Phys. Rev. B* **1994**, *50*, 17953–17979.
- (34) Yeh, J. J.; Lindau, I. Atomic Subshell Photoionization Cross Sections and Asymmetry Parameters: 1 [Less-than-or-Equals, Slant] Z [Less-than-or-Equals, Slant] 103. *At. Data Nucl. Data Tables* **1985**, *32*, 1–155.
- (35) Savory, C. N.; Ganose, A. M.; Travis, W.; Atri, R. S.; Palgrave, R. G.; Scanlon, D. O. An Assessment of Silver Copper Sulfides for Photovoltaic Applications: Theoretical and Experimental Insights. *J. Mater. Chem. A* **2016**, *4*, 12648–12657.
- (36) Bhachu, D. S.; Moniz, S. J. A.; Sathasivam, S.; Scanlon, D. O.; Walsh, A.; Bawaked, S. M.; Mokhtar, M.; Obaid, A. Y.; Parkin, I. P.; Tang, J.; Carmalt, C. J. Bismuth Oxyhalides: Synthesis, Structure and Photoelectrochemical Activity. *Chem. Sci.* **2016**, *7*, 4832–4841.
- (37) Sathasivam, S.; Arnepalli, R. R.; Bhachu, D. S.; Lu, Y.; Buckeridge, J.; Scanlon, D. O.; Kumar, B.; Singh, K. K.; Visser, R. J.; Blackman, C. S.; Carmalt, C. J. Single Step Solution Processed GaAs Thin Films from GaMe₃ and T BuAsH₂ under Ambient Pressure. *J. Phys. Chem. C* **2016**, *120*, 7013–7019.
- (38) Williamson, B. A. D.; Buckeridge, J.; Brown, J.; Ansbro, S.; Palgrave, R. G.; Scanlon, D. O. Engineering Valence Band Dispersion for High Mobility P-

- Type Semiconductors. *Chem. Mater.* **2017**, *29*, 2402–2413.
- (39) Mills, A.; Wang, J. Simultaneous Monitoring of the Destruction of Stearic Acid and Generation of Carbon Dioxide by Self-Cleaning Semiconductor Photocatalytic Films. *J. Photochem. Photobiol. A Chem.* **2006**, *182*, 181–186.
- (40) Mills, A.; McFarlane, M. Current and Possible Future Methods of Assessing the Activities of Photocatalyst Films. *Catal. Today* **2007**, *129*, 22–28.
- (41) Crick, C. R.; Parkin, I. P. CVD of Copper and Copper Oxide Thin Films via the in Situ Reduction of Copper(ii) Nitrate—a Route to Conformal Superhydrophobic Coatings. *J. Mater. Chem.* **2011**, *21*, 14712–14716.
- (42) Li, J.; Tang, C.; Li, D.; Haneda, H.; Ishigaki, T. Monodispersed Spherical Particles of Brookite-Type TiO₂: Synthesis, Characterization, and Photocatalytic Property. *J. Am. Ceram. Soc.* **2004**, *87*, 1358–1361.
- (43) Hu, W.; Li, L.; Li, G.; Tang, C.; Sun, L. High-Quality Brookite TiO₂ Flowers: Synthesis, Characterization, and Dielectric Performance. *Cryst. Growth Des.* **2009**, *9*, 3676–3682.
- (44) Pottier, A.; Chanéac, C.; Tronc, E.; Mazerolles, L.; Jolivet, J.-P. Synthesis of Brookite TiO₂ Nanoparticles by Thermolysis of TiCl₄ in Strongly Acidic Aqueous Media. *J. Mater. Chem.* **2001**, *11*, 1116–1121.
- (45) Mittal, K. L. Adhesion Measurement of Thin Films. *Electrocompon. Sci. Technol.* **1976**, *3*, 21–42.
- (46) Wyckoff, R. *Crystal Structures*; Wiley (New York): New York, 1963.
- (47) Di Paola, A.; Bellardita, M.; Palmisano, L. Brookite, the Least Known TiO₂ Photocatalyst. *Catalysts* **2013**, *3*, 36–73.
- (48) Tompsett, G. A.; Bowmaker, G. A.; Cooney, R. P.; Metson, J. B.; Rodgers, K. A.; Seakins, J. M. The Raman Spectrum of Brookite, TiO₂ (PBCA, Z= 8). *J. Raman Spectrosc.* **1995**, *26*, 57–62.
- (49) Iliev, M. N.; Hadjiev, V. G.; Litvinchuk, A. P. Raman and Infrared Spectra of Brookite (TiO₂): Experiment and Theory. *Vib. Spectrosc.* **2013**, *64*, 148–152.

- (50) Ohsaka, T.; Izumi, F.; Fujiki, Y. Raman Spectrum of Anatase, TiO₂. *J. Raman Spectrosc.* **1978**, *7*, 321–324.
- (51) Ponja, S.; Sathasivam, S.; Chadwick, N.; Kafizas, A.; Bawaked, S. M.; Obaid, A. Y.; Al-Thabaiti, S.; Basahel, S. N.; Parkin, I. P.; Carmalt, C. J. Aerosol Assisted Chemical Vapour Deposition of Hydrophobic TiO₂-SnO₂ Composite Film with Novel Microstructure and Enhanced Photocatalytic Activity. *J. Mater. Chem. A* **2013**, *1*, 6271–6278.
- (52) Koelsch, M.; Cassaignon, S.; Guillemoles, J. .; Jolivet, J. . Comparison of Optical and Electrochemical Properties of Anatase and Brookite TiO₂ Synthesized by the Sol–gel Method. *Thin Solid Films* **2002**, *403–404*, 312–319.
- (53) Kandiel, T. A.; Feldhoff, A.; Robben, L.; Dillert, R.; Bahnemann, D. W. Tailored Titanium Dioxide Nanomaterials: Anatase Nanoparticles and Brookite Nanorods as Highly Active Photocatalysts. *Chem. Mater.* **2010**, *22*, 2050–2060.
- (54) Grätzel, M.; Rotzinger, F. P. The Influence of the Crystal Lattice Structure on the Conduction Band Energy of Oxides of titanium(IV). *Chem. Phys. Lett.* **1985**, *118*, 474–477.
- (55) Zhu, T.; Gao, S.-P. The Stability, Electronic Structure, and Optical Property of TiO₂ Polymorphs. *J. Phys. Chem. C* **2014**, *118*, 11385–11396.
- (56) Pan, H.; Qiu, X.; Ivanov, I. N.; Meyer, H. M.; Wang, W.; Zhu, W.; Paranthaman, M. P.; Zhang, Z.; Eres, G.; Gu, B. Fabrication and Characterization of Brookite-Rich, Visible Light-Active TiO₂ Films for Water Splitting. *Appl. Catal. B Environ.* **2009**, *93*, 90–95.
- (57) Mills, A.; Le Hunte, S. An Overview of Semiconductor Photocatalysis. *J. Photochem. Photobiol. A Chem.* **1997**, *108*, 1–35.
- (58) Park, J.-J.; Kim, D.-Y.; Latthe, S. S.; Lee, J.-G.; Swihart, M. T.; Yoon, S. S. Thermally Induced Superhydrophilicity in TiO₂ Films Prepared by Supersonic Aerosol Deposition. *ACS Appl. Mater. Interfaces* **2013**, *5*, 6155–6160.
- (59) Peng, B.; Tan, L.; Chen, D.; Meng, X.; Tang, F. Programming Surface Morphology of TiO₂ Hollow Spheres and Their Superhydrophilic Films. *ACS*

Appl. Mater. Interfaces **2011**, *4*, 96–101.

- (60) Houmard, M.; Riassetto, D.; Roussel, F.; Bourgeois, A.; Berthomé, G.; Joud, J. C.; Langlet, M. Enhanced Persistence of Natural Super-Hydrophilicity in TiO₂-SiO₂ Composite Thin Films Deposited via a Sol-gel Route. *Surf. Sci.* **2008**, *602*, 3364–3374.
- (61) Kafizas, A.; Godin, R.; Durrant, J. R. Charge Carrier Dynamics in Metal Oxide Photoelectrodes for Water Oxidation. In *Semiconductors and Semimetals*; Mi, Z., Wang, L., Jagadish, C., Eds.; UK: Academic Press, 2017; Vol. 97, pp 3–46.
- (62) Wang, X.; Kafizas, A.; Li, X.; Moniz, S. J. A.; Reardon, P. J. T.; Tang, J.; Parkin, I. P.; Durrant, J. R. Transient Absorption Spectroscopy of Anatase and Rutile: The Impact of Morphology and Phase on Photocatalytic Activity. *J. Phys. Chem. C* **2015**, *119*, 10439–10447.
- (63) Guzman, F.; Chuang, S. S. C.; Yang, C. Role of Methanol Sacrificing Reagent in the Photocatalytic Evolution of Hydrogen. *Ind. Eng. Chem. Res.* **2013**, *52*, 61–65.
- (64) Moss, B.; Lim, K. K.; Beltram, A.; Moniz, S.; Tang, J.; Fornasiero, P.; Barnes, P.; Durrant, J.; Kafizas, A. Comparing Photoelectrochemical Water Oxidation, Recombination Kinetics and Charge Trapping in the Three Polymorphs of TiO₂. *Sci. Rep.* **2017**, *7*, 2938.
- (65) Kafizas, A.; Wang, X.; Pendlebury, S. R.; Barnes, P. R. F.; Ling, M.; Sotelo-Vazquez, C.; Quesada-Cabrera, R.; Li, C.; Parkin, I. P.; Durrant, J. R. Where Do Photo-Generated Holes Go in Anatase:Rutile TiO₂? A Transient Absorption Spectroscopy Study of Charge Transfer and Lifetime. *J. Phys. Chem. A* **2016**, *120*, 715–723.
- (66) Vequizo, J. J. M.; Matsunaga, H.; Ishiku, T.; Kamimura, S.; Ohno, T.; Yamakata, A. Trapping-Induced Enhancement of Photocatalytic Activity on Brookite TiO₂ Powders: Comparison with Anatase and Rutile TiO₂ Powders. *ACS Catal.* **2017**, *7*, 2644–2651.
- (67) Peiró, A. M.; Colombo, C.; Doyle, G.; Nelson, J.; Mills, A.; Durrant, J. R. Photochemical Reduction of Oxygen Adsorbed to Nanocrystalline TiO₂ Films:

A Transient Absorption and Oxygen Scavenging Study of Different TiO₂ Preparations. *J. Phys. Chem. B* **2006**, *110*, 23255–23263.

- (68) Kafizas, A.; Kellici, S.; Darr, J. A.; Parkin, I. P. Titanium Dioxide and Composite Metal/metal Oxide Titania Thin Films on Glass: A Comparative Study of Photocatalytic Activity. *J. Photochem. Photobiol. A Chem.* **2009**, *204*, 183–190.

ToC

